Supporting Information

Effective Orange-Red Solution-Processed Circularly Polarized Organic Light-Emitting Diode

Junqing Wang,[a] Xiaoyi Lai,[a] Yongzhi Zhou,[a,b] Lei Hua,[a] Weiguo Zhu,[a] Pengfei Duan,[b]* Yafei Wang[a]*

[a]School of Materials Science & Engineering, Jiangsu Collaborative Innovation Center of Photovoltaic Science and Engineering, Jiangsu Engineering Laboratory of Light-Electricity-Heat Energy-Converting Materials and Applications, Changzhou University, Changzhou 213164, PR China. Email: Y. Wang: qiji830404@hotmail.com

[b]CAS Key Laboratory of Nanosystem and Hierarchical Fabrication, National Center for Nanoscience and Technology (NCNST), No.11, ZhongGuanCun BeiYiTiao, Beijing 100190, P. R. China. P. Duan: E-mail: duanpf@nanoctr.cn

Table of Contents

General Informations 2

Theoretical Calculations 3

Device Fabrication and Characterization 3

Materials and Methods 4

Synthesis and Characterization 4

Thermal properties 15

Electrochemical property 15

Theoretical calculation 16

Photophysical properties 17

Electroluminescence performances 18

General Informations

^{1}H and ^{13}C nuclear magnetic resonance (NMR) spectra were acquired using a Bruker Dex-400 NMR spectrometer at room temperature, employing $CDCl_3$ or DMSO as solvents and tetramethyl silane as an internal standard. The NMR chemical shifts are reported in ppm with reference to residual protons and carbons of $CDCl_3$ (δ 7.26 ppm in ^{1}H NMR, δ 77.16 ppm in ^{13}C NMR), DMSO (δ 2.62 ppm in ^{1}H NMR, δ 39.52 ppm in ^{13}C NMR). Mass spectra (MS) were recorded on a Bruker Autoflex MALDI-TOF instrument using dithranol as a matrix. Thermogravimetric analysis (TGA) was detected with a NETZSCH STA449 from 25 °C to 600 °C at a 20 °C/min heating rate under N_2 atmosphere. The degradation temperature (T_d) was determined based on the 5% weight loss. Differential scanning calorimetry (DSC) was performed on a TAQ2000 differential scanning calorimeter at a heating rate of 10 °C min^{-1} from 30 to 300 °C under nitrogen atmosphere. Cyclic voltammetry measurements were performed using a 273 A (Princeton Applied Research). Electrochemical property was evaluated by cyclic voltammetry with three typical electrodes in degassed CH3CN solution with a rate of 100 mV/s. The CV system employed Bu4NPF6 as electrolyte. Platinum disk was used as the working electrode, platinum wire was regarded as the counter electrode and silver wire was used as the reference electrode. Ferrocenium/ferrocene (Fc/Fc^{+}) was used as the external standard compound. Each oxidation potential was calibrated using ferrocene as a reference.

UV-visible absorption spectra were recorded on a Shimadzu UV-2600. Steady-state and transient-state PL spectra, photoluminescence quantum yield (PLQY) and lifetime were carried out by using an Edinburgh FLS1000 Photoluminescence Spectrometer. Circular dichroism (CD) was measured on a Jasco J-1500 CD Sepctrometer. Circularly polarized photoluminescence (CPPL) and electroluminescence (CPEL) spectra were measured on a Jasco CPL-200 spectrometer. The test mode adopted the "Slit" mode with the E_x and E_m Slit width set at 3000 μm, and the digital integration time (D.I.T.) was set at 2.0 s with multiple accumulations.

Theoretical Calculations

Density functional theory (DFT) computations encompassing geometrical optimization and electronic properties evaluations of these chiral thermally activated delayed fluorescence (TADF) molecules at ground-states were conducted using the Gaussian 16 software package at the PBE1PBE/6-311g (d, p) level, The energy levels of the excited states were computed employing the time-dependent DFT (TD-DFT) method at the same PBE1PBE/6-311g (d, p) level. Spin-orbit coupling matrix element (SOCME) values between the S_1 and T_n (n = 1~4) states were calculated with ORCA 4.2.1 package at PBE0 /TZVP. Configuration optimization of the lowest singlet states (S_1) of these chiral molecules was executed through TD-DFT at the PBE1PBE/6-311g (d, p) level, with relevant parameters for circularly polarized photoluminescence (CPPL) being concurrently output. All calculations were performed in the gas phase and visualized using GaussView 6.0 or VMD 1.9.3.

Device Fabrication and Characterization

Poly(styrenesulfonate) (PEDOT: PSS) was purchased from Xi'an Polymer Light Technology Corp. TCTA (4,4',4''-Tris(carbazol-9-yl)-triphenylamine), PVK (Poly(N-vinylcarbazole),DtBuCzB (Indolo[3,2,1de]indolo[3',2',1':8,1][1,4]benzazaborino[2,3,4-kl]phenazaborine,2,5,15,18-tetrakis(1,1-dimethylethyl), DPEPO (Bis[2 (diphenylphosphino)phenyl]ether oxide) and (TmPyPB)1,3,5-tris[(3-pyridyl)phen3-yl]benzene, and LiF were purchased from Lumtec.

In devices, PEDOT: PSS was used as hole injection material. TCTA was used as host material. **(*R*)-ad-PXZ/(*S*)-ad-PXZ** were used as emission layer and DtBuCzB was used as sensitizer . PVK was used as hole transporting layer. TmPyPB, DPEPO and LiF were used as electron transport, hole blocking and injection materials respectively. (Indium tin oxide) (ITO) and (Aluminium) (Al) were used as anode and cathode materials respectively. All commercially available reagents were used without further purification.

The substrates were successively cleaned with isopropyl alcohol, acetone, detergent, deionized water, and isopropyl alcohol in an ultrasonic bath and then dried overnight in the oven.

The substrates pre-treated by oxygen plasma to increase the work function of the ITO film. Then, 35 nm-thick PEDOT: PSS was spin-coated onto the ITO substrates at 3200 rpm for 30 s and annealed at 150 °C for 15 min. And then emissive layer was spin coated and annealed at 60 °C for 30 min using a precursor containing different materials co-dissolved in chloroform or toluene. The films of DPEPO, TmPyPB, LiF and aluminum were prepared by thermal evaporation under a vacuum of 1×10^{-4} Pa. Each sample has an active area of 0.04 cm^2. All the devices were encapsulated before characterization to prevent degradation and emission quenching caused by oxygen and water. The EL spectra and J–V–L curves were obtained with a PHOTORESEARCH Spectra Scan PR735 photometer and a KEITHLEY 2400 Source Meter constant current source at room temperature. The EQE values were calculated by assuming a Lambertian distribution.

Materials and Methods

All the commercially available reagents and solvents used in this work were used directly unless otherwise mentioned. Chiral source of R/S [1,1'-binaphthalene]-2,2'-diamine, were purchased from Shanghai Daicel Corporation, All reagents used in the experiments were purchased from commercial sources without further purification. For column chromatography, silica gel with 200−300 mesh was used.

Synthesis and Characterization

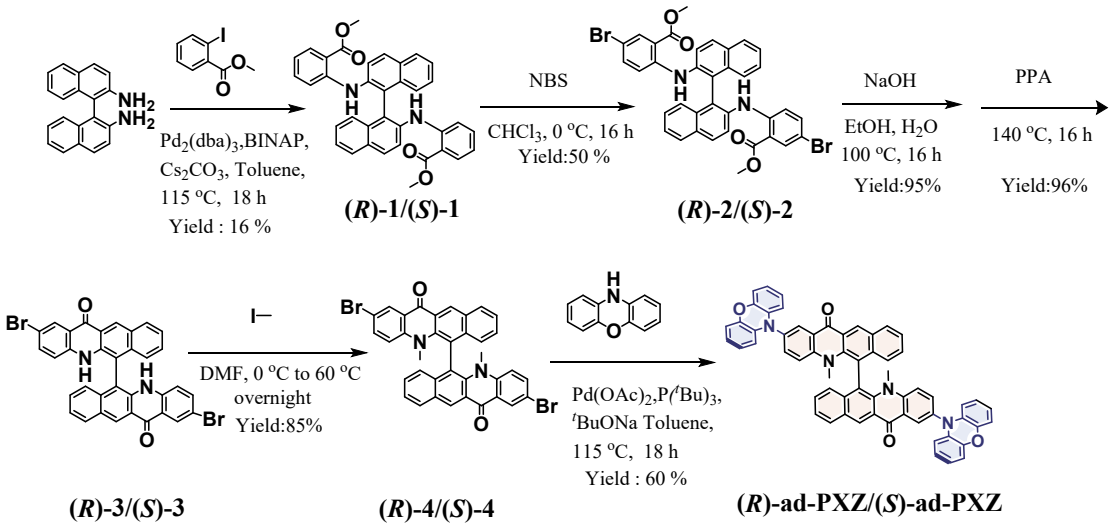

Scheme S1. Synthesis routes of of the **(*R*)-ad-PXZ/(*S*)-ad-PXZ.**

Synthesis of (*R*)-1/(*S*)-1: (*R*) -[1,1'-binaphthalene]-2,2'-diamine /(*S*)-[1,1'-binaphthalene]-2,2'-diamine (BINAM) (2.0 g, 7.0 mmol), methyl 2-iodobenzoate (5.5 g, 21.0 mmol), Tris(dibenzylideneacetone)dipalladium (384.9 mg, 0.4 mmol), 1.1'-Binaphthyl-2.2'-diphemyl phosphine (525.2 mg, 0.8 mmol) and Cesium carbonate (12.4 g, 35.1 mmol) were dissolved in anhydrous toluene (100.0 mL).The mixture was heated to 115 °C for 18 hours under a Nitrogen atmosphere. After cooling to room temperature, the mixture was extracted with dichloromethane. The combined organic layer was washed by saturated brine, then dried over anhydrous $MgSO_4$. The crude was purified by silica gel column (ethyl acetate/petroleum ether = 1/6, v/v) to give white powder of **(*R*)-1/(*S*)-1**.

For **(*R*)-1** (1.0 g, yield: 16 %): ^{1}H NMR (400 MHz, Chloroform-d) δ 8.65 (s, 2H), 7.91 (d, J = 8.9 Hz, 2H), 7.87 (d, J = 8.2 Hz, 2H), 7.77 (d, J = 8.9 Hz, 2H), 7.71 (dd, J = 7.9, 1.7 Hz, 2H), 7.35 (t, J = 8.1, 6.5, 1.5 Hz, 2H), 7.29 (d, J = 8.5 Hz, 2H), 7.24 – 7.18 (m, 4H), 7.13 – 7.08 (m, 2H), 6.63 – 6.58 (m, 2H), 3.41 (s, 6H) **(Fig S1)**.

For **(*S*)-1** (1.0 g, yield: 16 %): ^{1}H NMR (400 MHz, Chloroform-d) δ 8.64 (s, 2H), 7.91 (d, J = 8.9 Hz, 2H), 7.87 (d, J = 8.2 Hz, 2H), 7.76 (d, J = 8.9 Hz, 2H), 7.71 (d, J = 8.0 Hz, 2H), 7.35 (t, J = 7.4 Hz, 2H), 7.28 (d, J = 8.5 Hz, 2H), 7.23 (d, J = 6.6 Hz, 2H), 7.19 (d, J = 8.4 Hz, 2H), 7.12 – 7.08 (m, 2H), 6.60 (t, J = 7.6 Hz, 2H), 3.41 (s, 6H) **(Fig S2)**.

Synthesis of (*R*)-2/(*S*)-2: To a colourless solution of NBS (643.5 mg, 2.8 mmol, 2 equivalents) in Trichloromethane ($CHCl_3$) (20.0 mL) was added a yellow solution of **(*R*)-**

1/(*S*)-1 (1.0 g, 1.8 mmol) in $CHCl_3$ (5.0 mL). The colourless solution immediately turned bright yellow. After stirring from 0 °C to the room temperature for 16 h in the dark and under a Nitrogen atmosphere, the mixture was extracted with dichloromethane. The combined organic layer was washed by saturated brine, then dried over anhydrous $MgSO_4$. This was followed by recrystallization with $CHCl_3$ and ethanol (EtOH). The product was obtained as yellow solid.

For **(*R*)-2** (600.0 mg, yield: 50 %): ^{1}H NMR (400 MHz, Chloroform-d) δ 8.67 (s, 2H), 7.94 (d, J = 8.9 Hz, 2H), 7.91 (d, J = 8.1 Hz, 2H), 7.83 (d, J = 2.5 Hz, 2H), 7.67 (d, J = 8.9 Hz, 2H), 7.42 (ddd, J = 8.1, 6.8, 1.3 Hz, 2H), 7.30 – 7.27 (m, 2H), 7.19 (d, J = 8.4 Hz, 2H), 7.12 (dd, J = 9.0, 2.5 Hz, 2H), 7.02 (d, J = 9.0 Hz, 2H), 3.48 (s, 6H) **(Fig S3)**.

For **(*S*)-2** (600.0 mg, yield: 50 %): ^{1}H NMR (400 MHz, Chloroform-d) δ 8.67 (s, 2H), 7.94 (d, J = 8.9 Hz, 2H), 7.91 (d, J = 8.1 Hz, 2H), 7.82 (d, J = 2.5 Hz, 2H), 7.67 (d, J = 8.8 Hz, 2H), 7.44 – 7.39 (m, 2H), 7.29 (d, J = 8.5 Hz, 2H), 7.19 (d, J = 8.5 Hz, 2H), 7.12 (dd, J = 9.1, 2.5 Hz, 2H), 7.02 (d, J = 9.0 Hz, 2H), 3.48 (s, 6H) **(Fig S4)**.

Synthesis of (***R*)-3/(*S*)-3: (R)-2/(S)-2** (580.0 mg, 1.2 mmol) and Sodium hydroxide (1.3 g, 23.7 mmol) were dissolved in the mixture of EtOH (10.0 mL) and distilled water (10.0 mL). After the reaction was heated to 100 °C for 12 hours. After the reaction colling to room temperature, hydrochloric acid (1.0 mol L^{-1}) was used to neutralize the solution. The solid was filtered and washed with water and petroleum ether. Yellow solid was acquired through drying. Subsequently, the yellow solid was added into a round-bottom flask, then polyphosphoric acid (PPA) was added until complete coverage of the yellow solid and stirred well with a spatula. The reaction mixture was stirred at 140 °C for 16 h. The resulting mixture was cooled to room temperature and poured into water. The precipitating solid of **(*R*)-3/(*S*)-3** was washed by distilled water and collected (520.0 mg, 96 %).

For (***R*)-3** (520.0 mg, yield: 96 %): ^{1}H NMR (400 MHz, DMSO-d6) δ 9.96 (s, 2H), 9.31 (s, 2H), 8.39 (d, J = 8.3 Hz, 2H), 8.34 (s, 2H), 7.70 (d, J = 8.9 Hz, 2H), 7.50 – 7.45 (m, 4H), 7.35 (t, J = 7.8 Hz, 2H), 6.84 (d, J = 8.7 Hz, 2H) **(Fig S5)**.

For **(*S*)-3** (520.0 mg, yield: 96 %): ^{1}H NMR (400 MHz, DMSO-d6) δ 9.98 (s, 2H), 9.30 (s, 2H), 8.38 (d, J = 8.2 Hz, 2H), 8.33 (s, 2H), 7.69 (d, J = 8.8 Hz, 2H), 7.48 (d, J = 8.5 Hz, 4H), 7.37 – 7.31 (t, J = 7.6 Hz 2H), 6.84 (d, J = 8.3 Hz, 2H) **(Fig S6)**.

Synthesis of (*R*)-**4/**(*S*)**-4:** (*R*)**-3**/(*S*)**-3** (700.0 mg, 1.1 mmol) was dissolved in dimethylformamide (10.0 mL) and cooled to 0 °C. Sodium hydride (347.6 mg, 8.6 mmol) was then added in portions while stirring. This was then heated to 60 °C and stirred for 30 mins at which point methyl iodide (1.2 g, 8.6 mmol) was added and stirred at 60 °C for 18 h. Upon completion, the reaction was cooled to ambient temperature and quenched with water. The solid was filtered via suction filtration and dissolved in dichloromethane then washed with a brine solution. The organic fractions were combined and dried over $MgSO_4$ with the volatiles being removed in vacuo to yield a flaky orange-red solid.

For **(*R*)-4** (520.0 mg**,** yield: 85 %**):** ^{1}H NMR (400 MHz, Chloroform-d) δ 9.27 (s, 2H), 8.51 (s, 2H), 8.22 (d, J = 8.7 Hz, 2H), 7.58 – 7.47 (m, 8H), 6.59 (d, J = 9.0 Hz, 2H), 2.49 (s, 6H) **(Fig S7)**.

For **(*S*)-4** (520.0 mg**,** yield: 85 %**):** ^{1}H NMR (400 MHz, Chloroform-d) δ 9.28 (s, 2H), 8.51 (s, 2H), 8.22 (d, J = 8.0 Hz, 2H), 7.58 – 7.47 (m, 8H), 6.59 (d, J = 9.0 Hz, 2H), 2.49 (s, 6H) **(Fig S8)**.

Synthesis of (*R*)-ad-PXZ/(*S*)-ad-PXZ: (*R*)-4/(*S*)-4 (300.0 mg, 0.4 mmol.), Phenoxazine (179.2 mg, 0.9 mmol), sodium tert-butoxide (213.5 mg, 2.2 mmol), Pd $(OAc)_2$ (5.9 mg, 0.02 mmol), $(tBu)_3P$ (26.9 mg, 0.1 mmol) and toluene (5.0 mL) were added to a 50.0 mL round-bottom flask. The mixture was stirred at 115 °C for 18 h under a nitrogen atmosphere. After cooling to room temperature, the mixture was poured into water and extracted with dichloromethane. The combined organic layers were washed with water, dried over anhydrous $MgSO_4$ and evaporated to dryness. The crude was purified by silica gel column (dichloromethane /petroleum ether = 3/1, v/v) to give orange-red powder of **(*R*)-ad-PXZ/(*S*)-ad-PXZ.**

For **(*R*)-4** (230.0 mg**,** yield: 60 %**):** ^{1}H NMR (400 MHz, Chloroform-d) δ 9.32 (s, 2H), 8.44 (s, 2H), 8.26 (d, J = 9.2 Hz, 2H), 7.67 (d, J = 7.1 Hz, 2H), 7.57 (td, J = 6.3, 5.9, 2.9

Hz, 4H), 7.40 (dd, J = 8.9, 2.5 Hz, 2H), 6.93 (d, J = 8.9 Hz, 2H), 6.67 (d, J = 7.9 Hz, 4H), 6.61 (t, J = 6.9 Hz, 4H), 6.51 (t, J = 7.7 Hz, 4H), 5.85 (d, J = 9.4 Hz, 4H), 2.62 (s, 6H). ^{13}C NMR (101 MHz, CDCl3) δ 179.67, 146.25, 143.33, 141.83, 138.01, 136.77, 136.68, 134.87, 133.87, 132.94, 132.10, 130.58, 130.22, 130.01, 129.82, 129.00, 126.34, 125.39, 124.60, 123.77, 122.99, 121.87, 120.61, 118.87, 115.40, 112.98, 41.17. MALDI-TOF (ESI) m/z calcd for $C_{60}H_{38}N_4O_4^+$ $[M+H]^+$ 878.2893, found 878.28856 **(Fig S9**, **S11** and **S13).**

For **(*S*)-4** (230.0 mg**,** yield:85 %**):** ^{1}H NMR (400 MHz, Chloroform-d) δ 9.32 (s, 2H), 8.44 (s, 2H), 8.26 (d, J = 6.9 Hz, 2H), 7.68 (d, J = 7.4 Hz, 2H), 7.56 (q, J = 7.1, 6.7 Hz, 4H), 7.40 (d, J = 8.9 Hz, 2H), 6.93 (d, J = 8.9 Hz, 2H), 6.68 (d, J = 7.9 Hz, 4H), 6.61 (t, J = 7.6 Hz, 4H), 6.51 (t, J = 7.7 Hz, 4H), 5.85 (d, J = 9.5 Hz, 4H), 2.63 (s, 6H). 13C NMR (101 MHz, CDCl3) δ 179.15, 143.80, 136.77, 136.24, 133.88, 132.11, 130.58, 130.23, 130.01, 129.83, 129.27, 125.86, 125.83, 125.40, 124.68, 123.62, 123.00, 121.46, 118.87, 115.41, 113.38, 112.98, 40.75. MALDI-TOF (ESI) m/z calcd for $C_{60}H_{38}N_4O_4^+$ $[M+H]^+$ 878.2893, found 878.28847 **(Fig S10**, **S12** and **S14).**

NMR and MS spectra

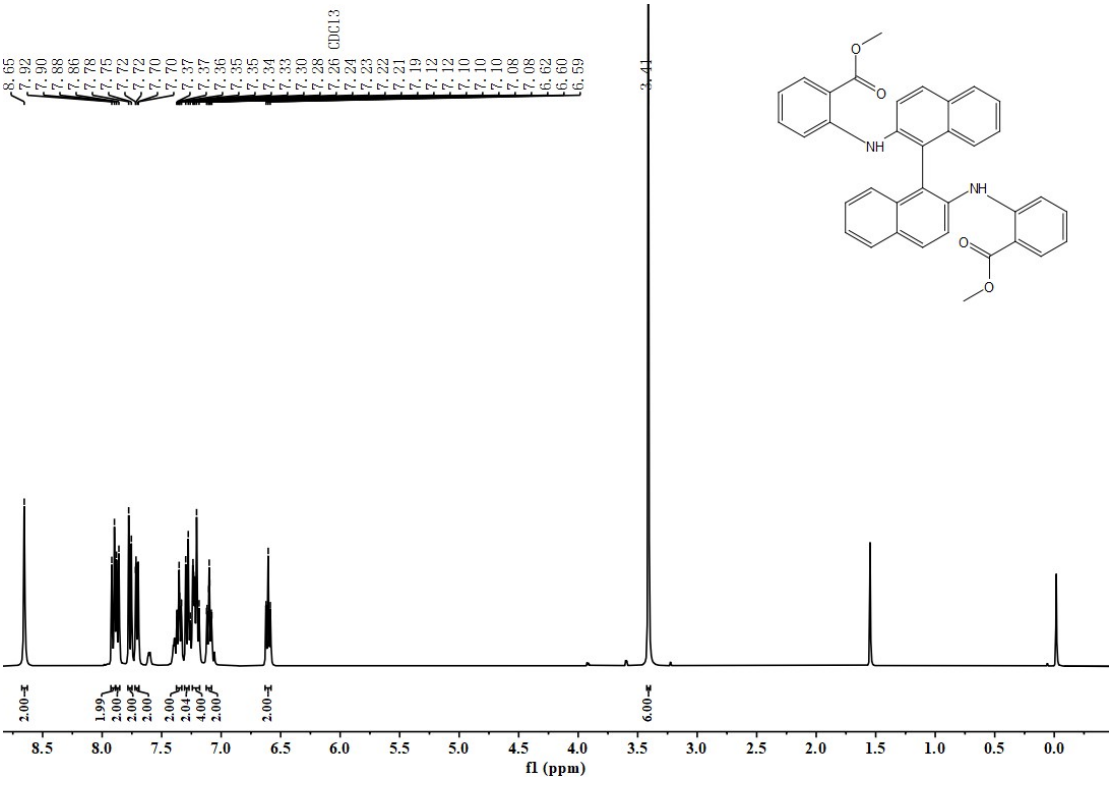

Fig S1. ^{1}H NMR spectrum of **(*R*)-1** in $CDCl_3$ at room temperature

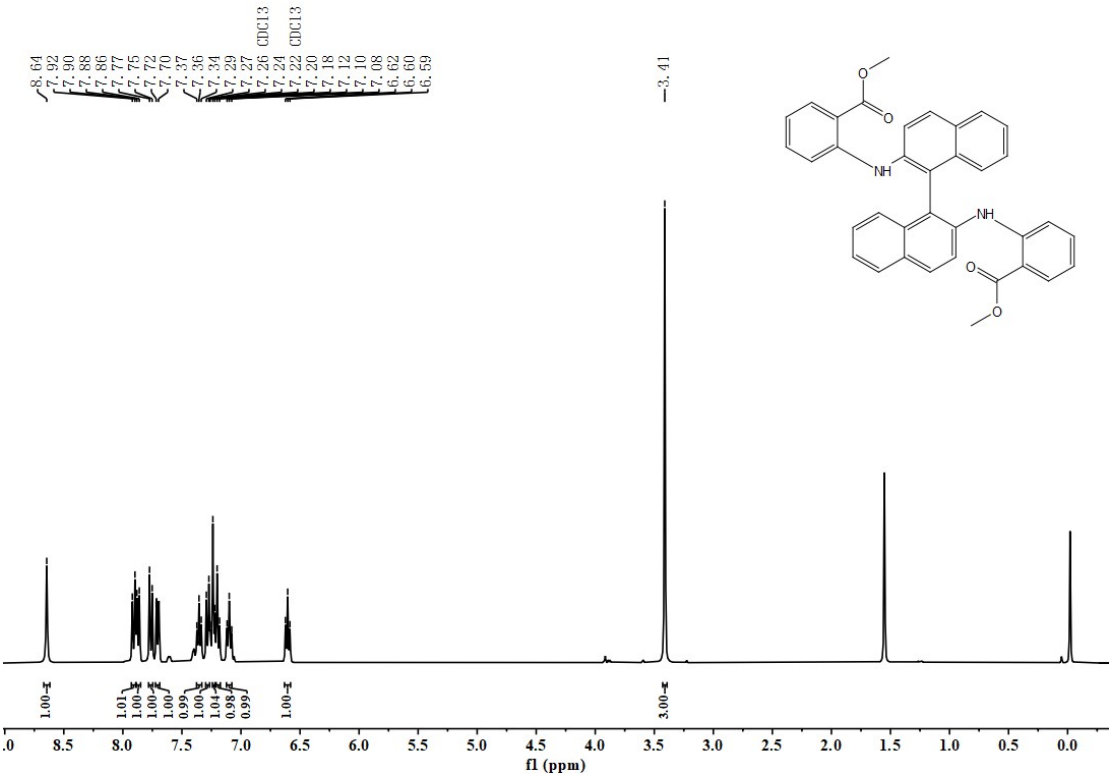

Fig S2. ^{1}H NMR spectrum of **(*S*)-1** in $CDCl_3$ at room temperature

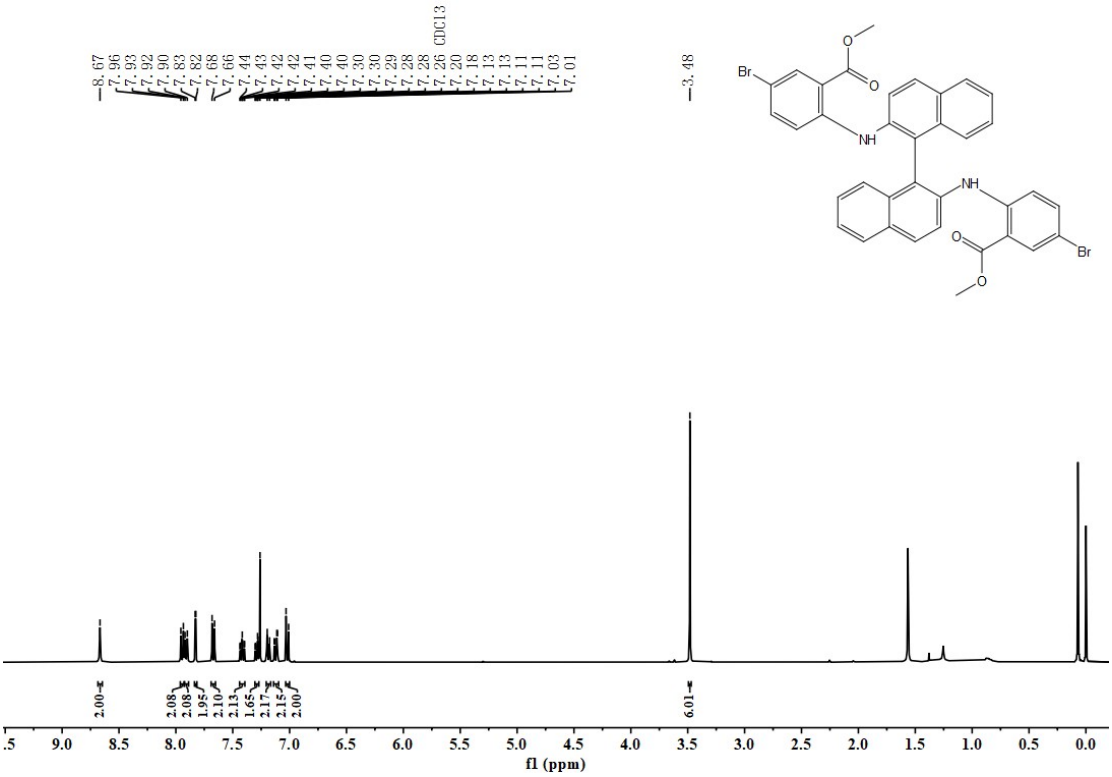

Fig S3. ^{1}H NMR spectrum of **(*R*)-2** in $CDCl_3$ at room temperature

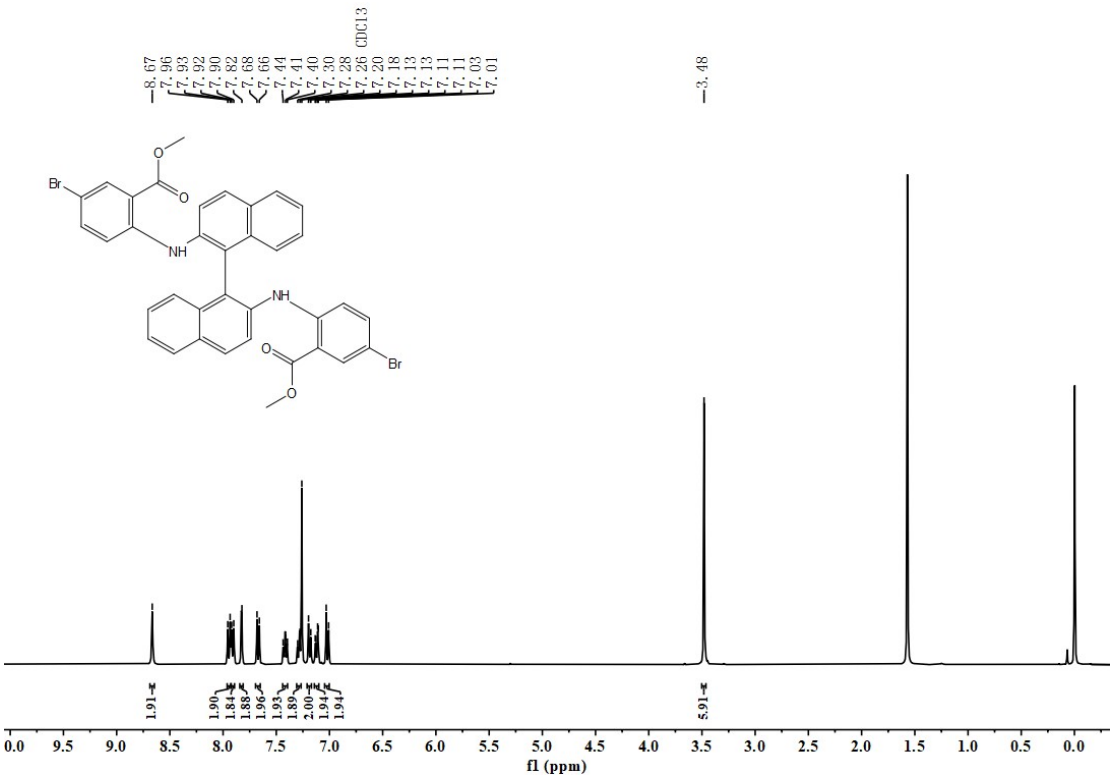

Fig S4. ^{1}H NMR spectrum of **(*S*)-2** in $CDCl_3$ at room temperature

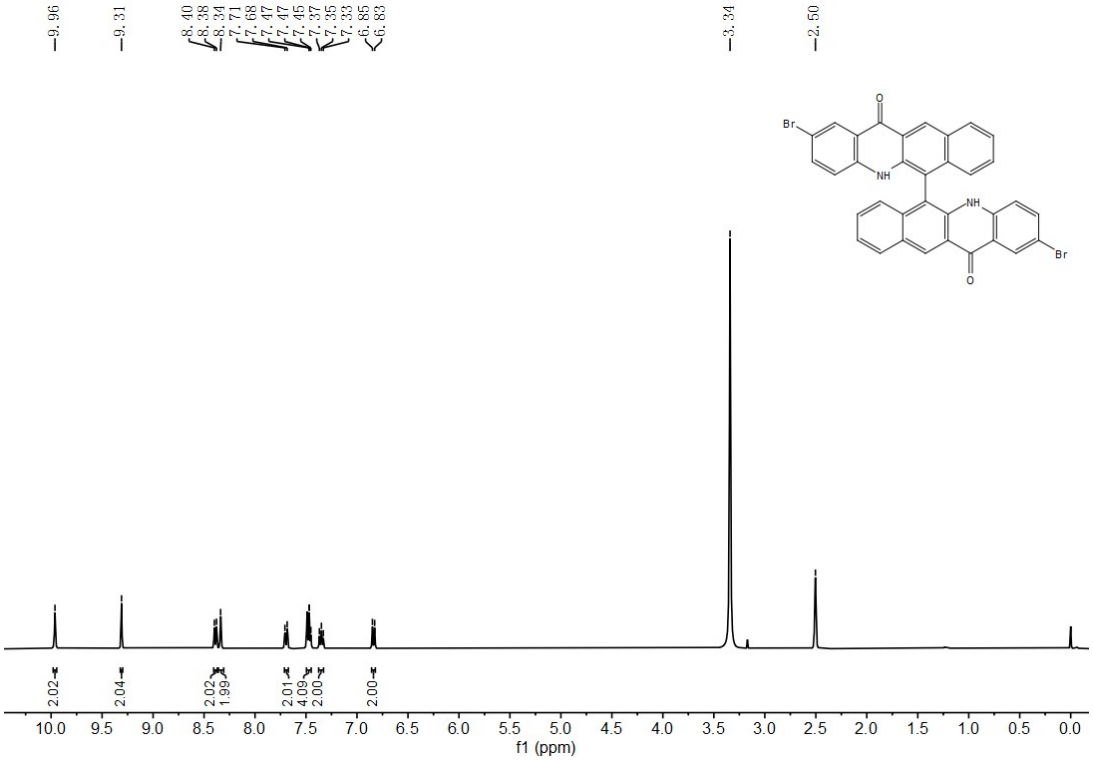

Fig S5. ^{1}H NMR spectrum of **(*R*)-3** in DMSO at room temperature

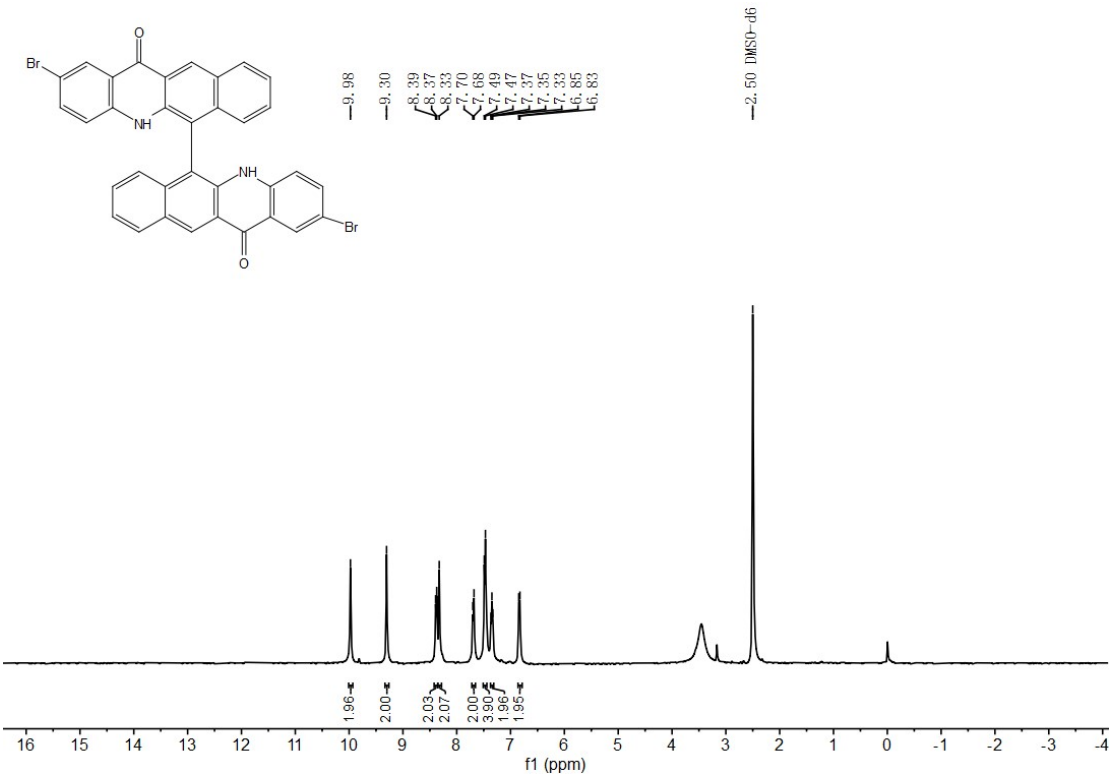

Fig S6. ^{1}H NMR spectrum of **(*S*)-3** in DMSO at room temperature

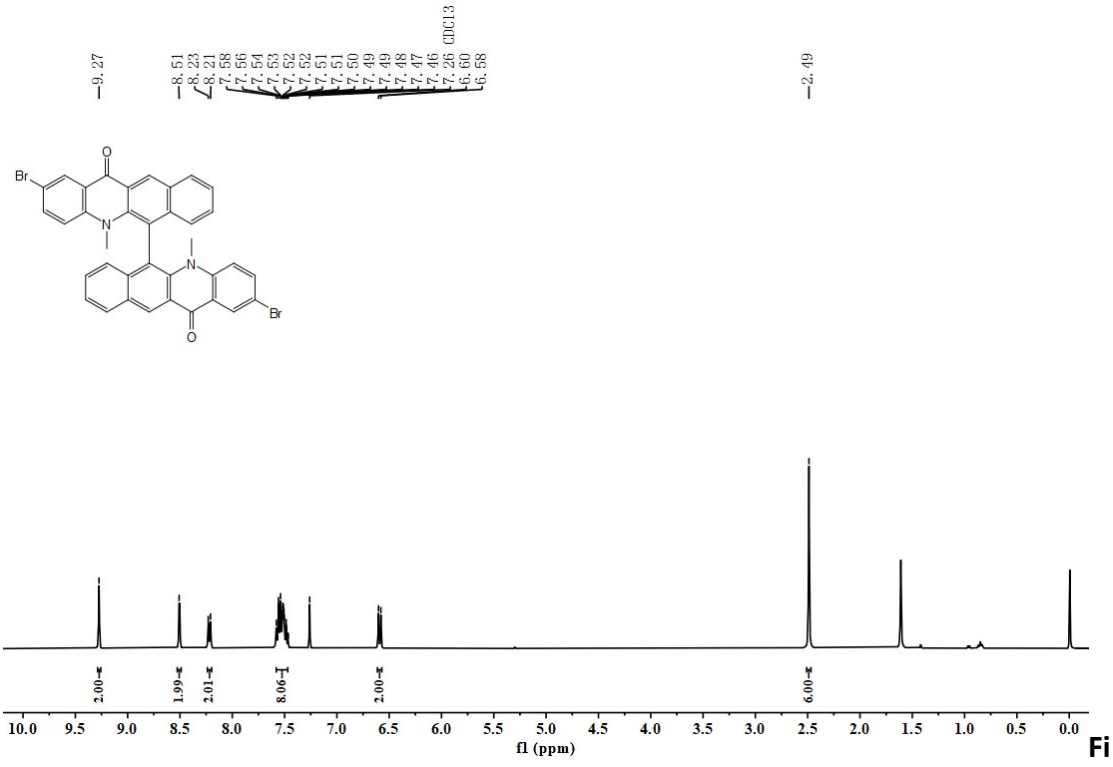

Fig S7. ^{1}H NMR spectrum of **(*R*)-4** in $CDCl_3$ at room temperature

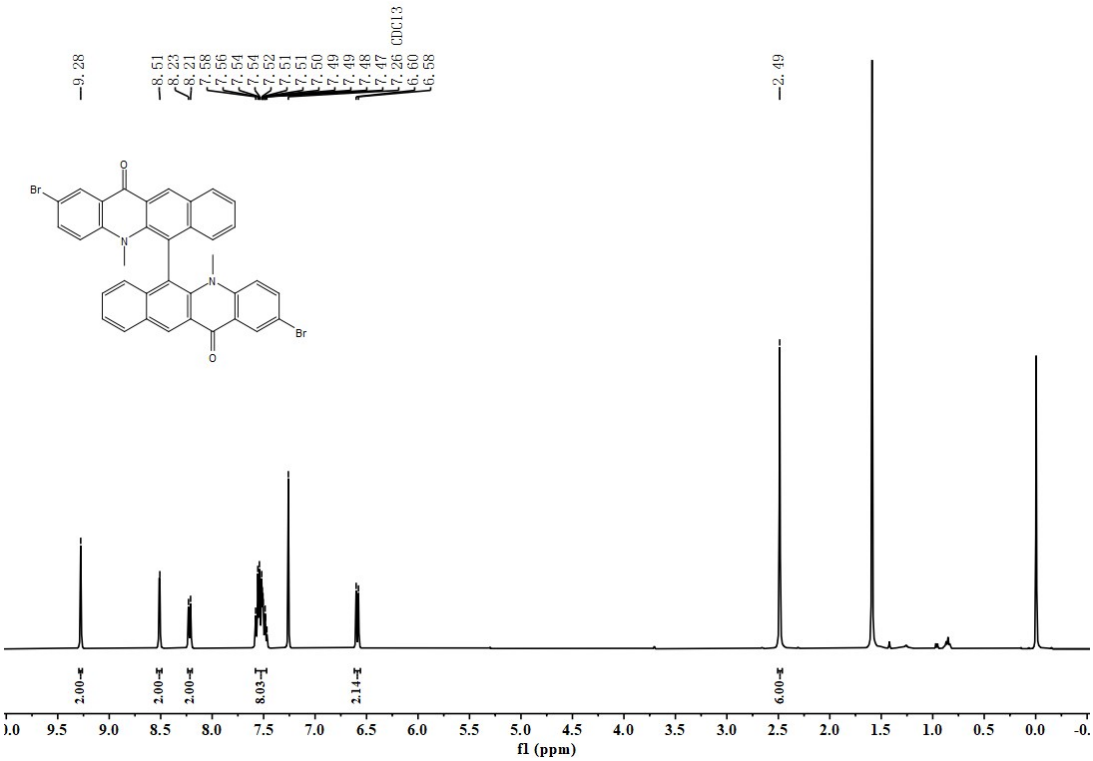

Fig S8. ^{1}H NMR spectrum of **(*S*)-4** in $CDCl_3$ at room temperature

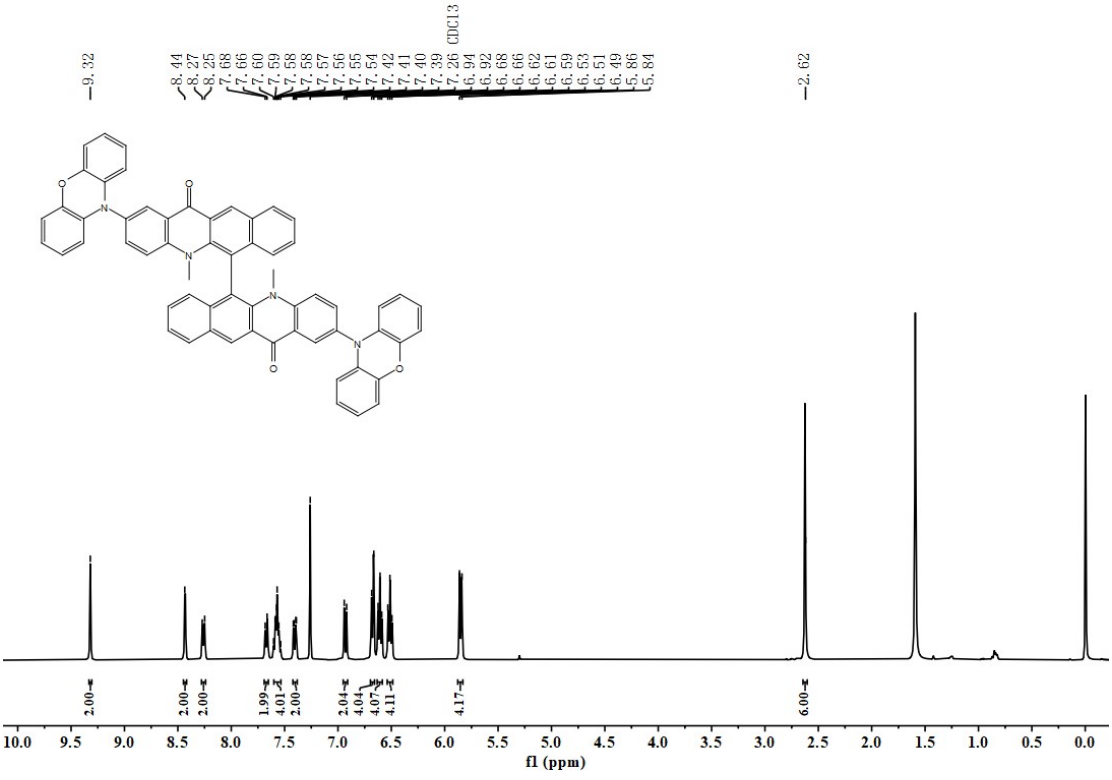

Fig S9. ^{1}H NMR spectrum of **(*R*)-ad-PXZ** in $CDCl_3$ at room temperature

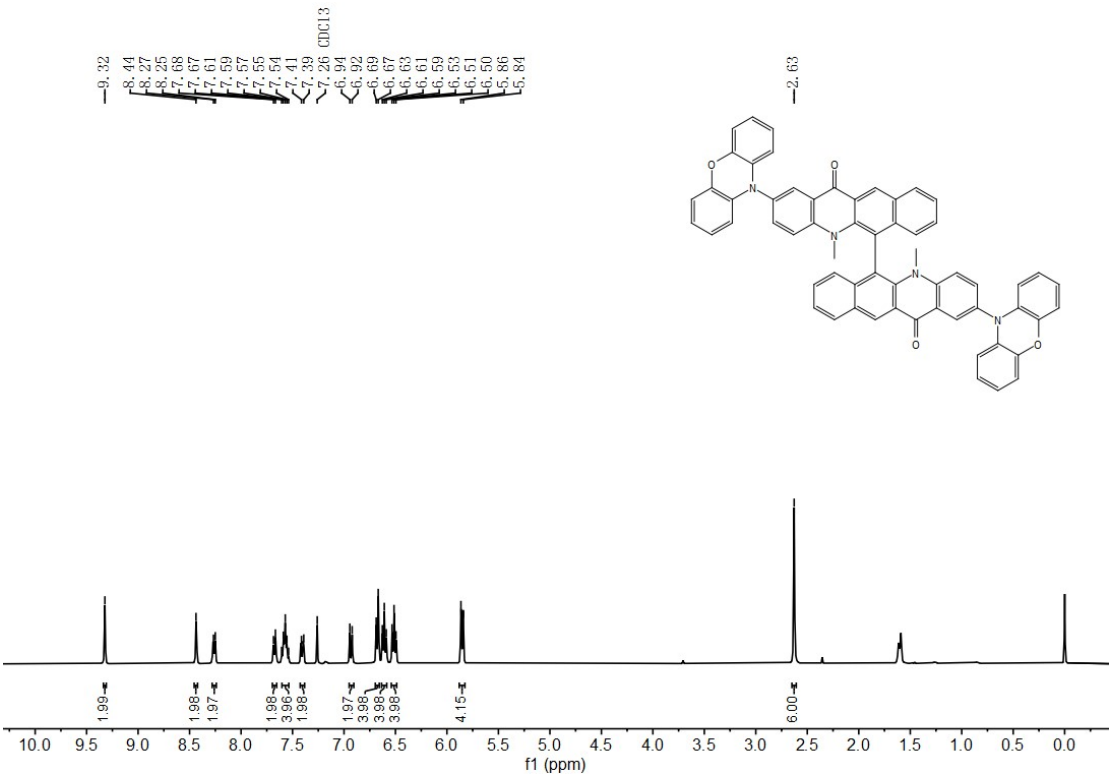

Fig S10. ^{1}H NMR spectrum of **(*S*)-ad-PXZ** in $CDCl_3$ at room temperature

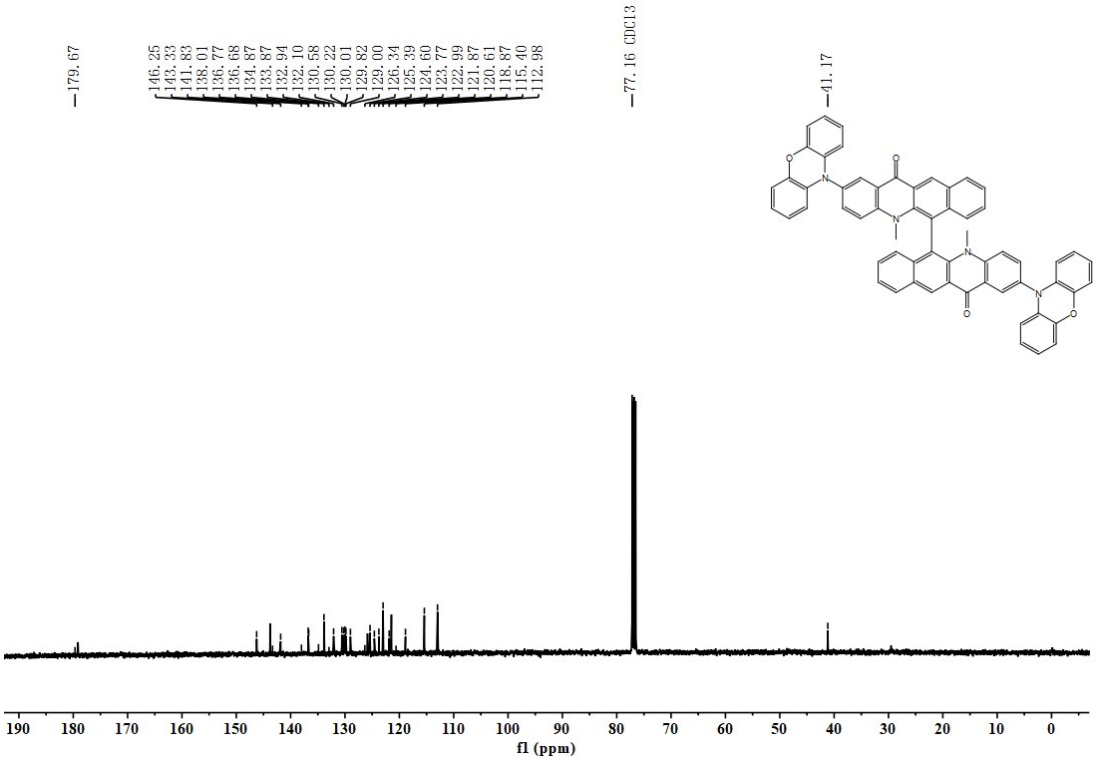

Fig S11. ^{13}C NMR spectrum of **(*R*)-ad-PXZ** in $CDCl_3$ at room temperature

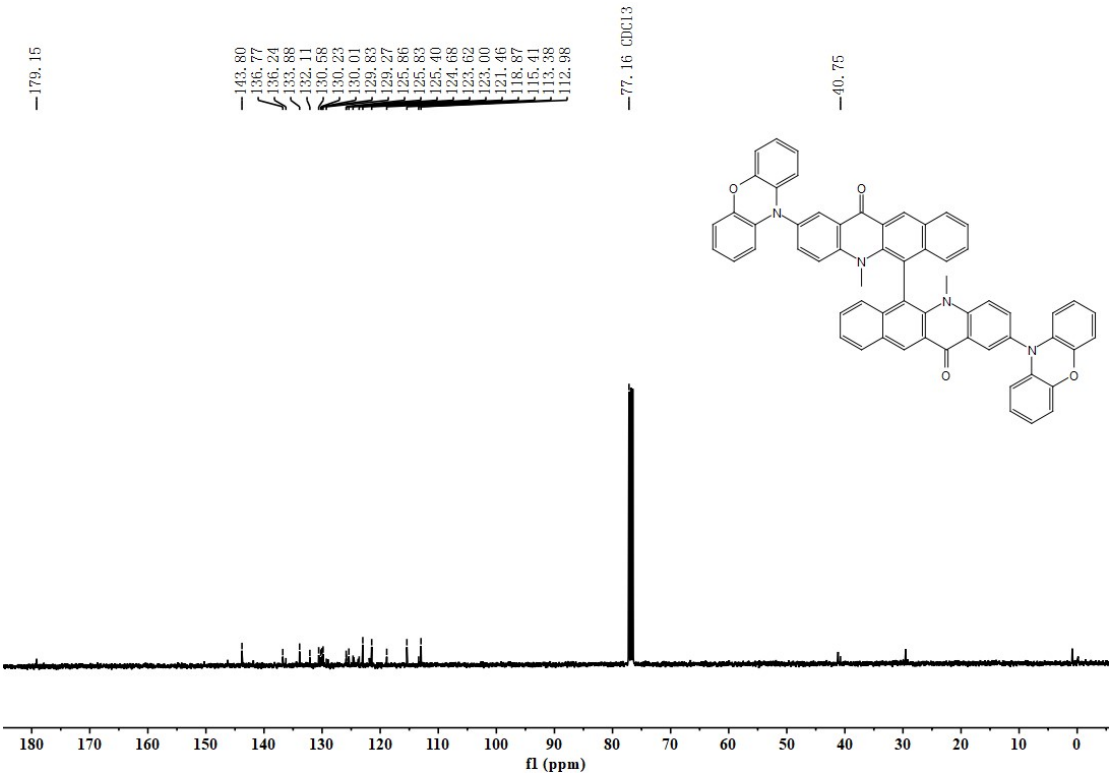

Fig S12. ^{13}C NMR spectrum of **(*S*)-ad-PXZ** in $CDCl_3$ at room temperature

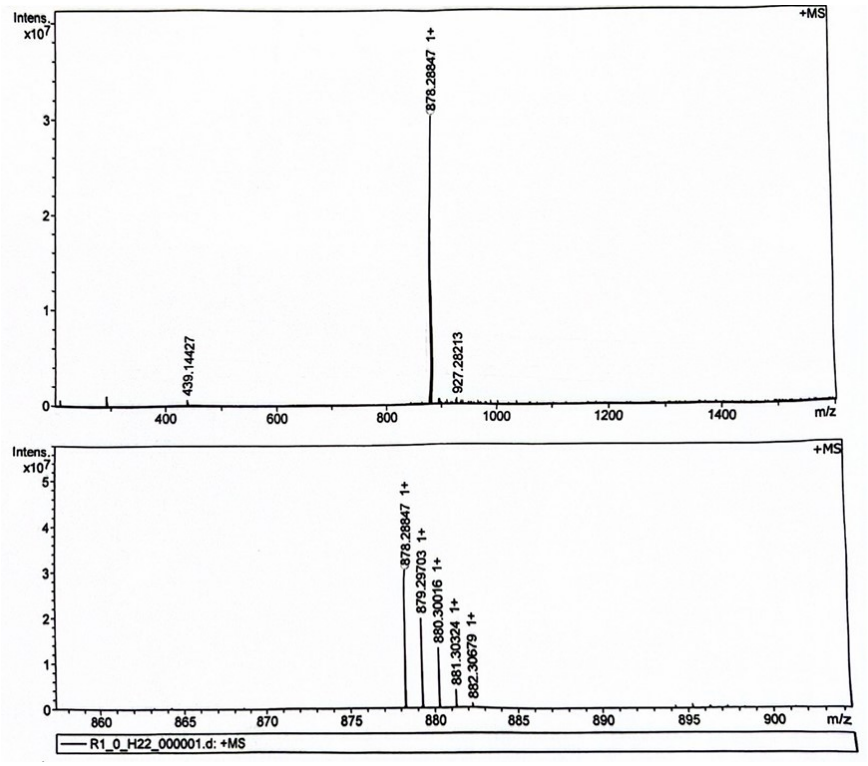

Fig S13. TOF-MS spectrum of **(*R*)-ad-PXZ** in $CDCl_3$ at room temperature

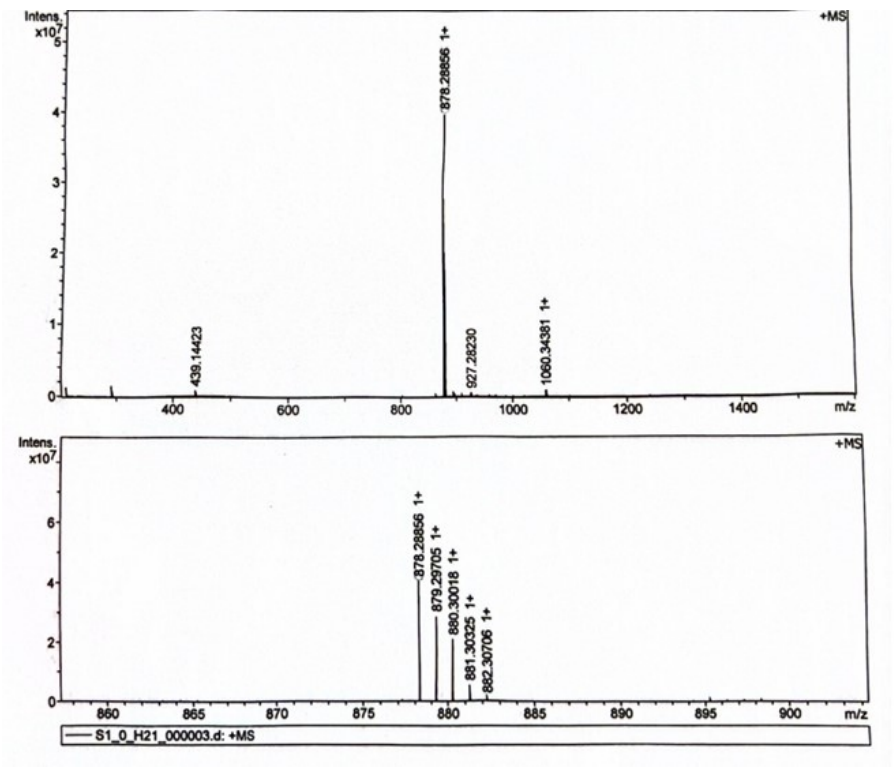

Fig S14. TOF-MS spectrum of **(*S*)-ad-PXZ** in $CDCl_3$ at room temperature

Thermal properties

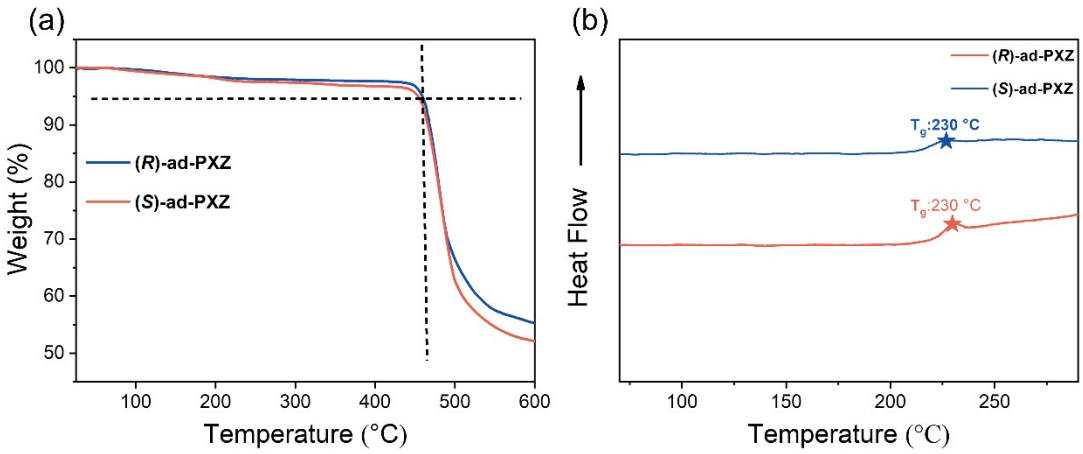

Fig S15. (a) TGA and (b) DSC curves of the **(*R*)-ad-PXZ** and **(*S*)-ad-PXZ.**

Electrochemical property

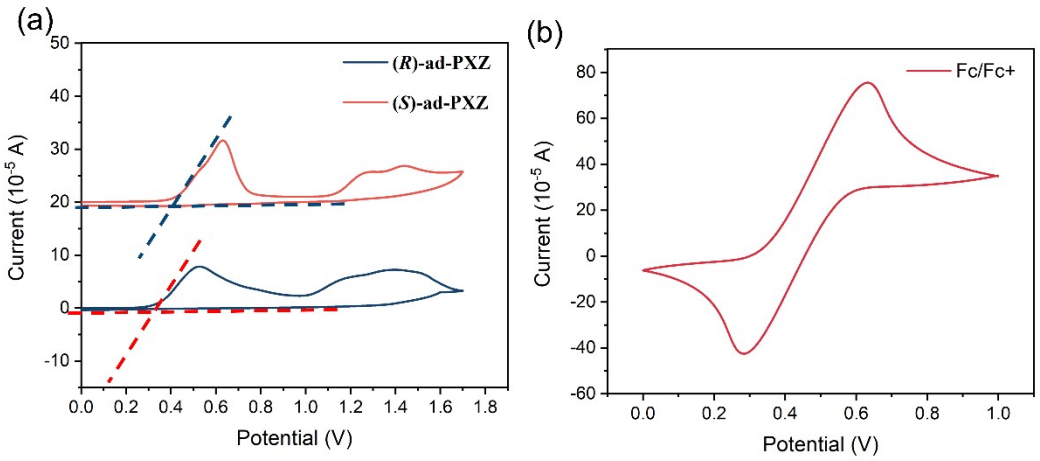

Fig S16. CV curves of the **(*R*)-ad-PXZ** and **(*S*)-ad-PXZ.**

Theoretical calculation

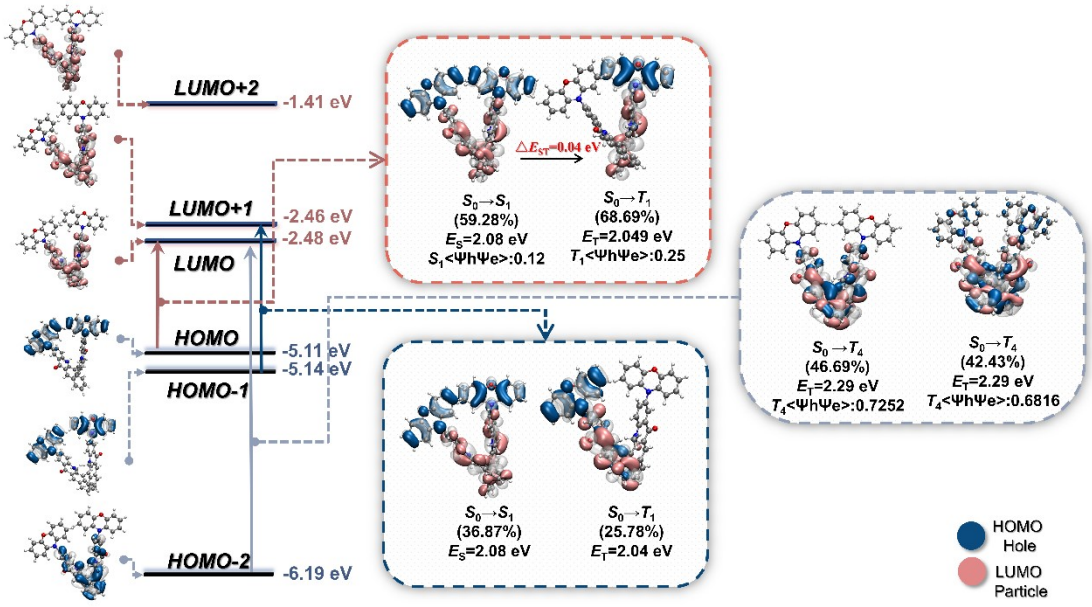

Fig S17. Theoretical simulation of ground and excited states for **(*R*)-ad-PXZ.** Contours and energy levels of the first FMOs for ground-state (S_0) **(*R*)-ad-PXZ** and their contributions to the singlet and triple excitations(S_1, T_1, T_4). HOMO and LUMO refer to the highest occupied and lowest unoccupied molecular orbitals, respectively. Contours of "hole" and "particle" and transition parameters for these excitations simulated with natural transition orbital (NTO) analysis (center in boxes). E, and $<\Psi_h\Psi_e>$ refer to excited-state energy level, the overlap integral, respectively. The subscripts of S and T refer to singlet and triplet states, respectively.

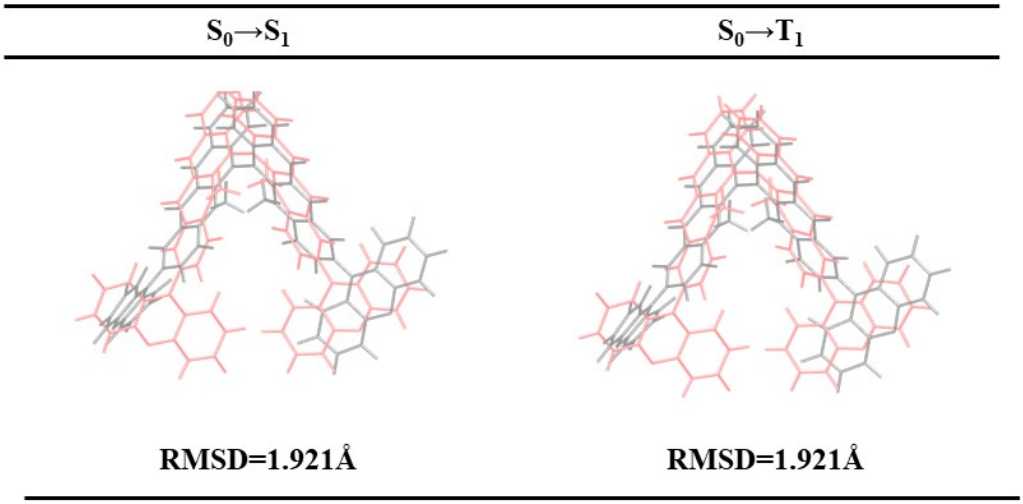

Fig S18. Configuration deviations between the S_0 (gray), S_1 (pink) and T_1 (pink) states of **(*R*)-ad-PXZ**

Photophysical properties

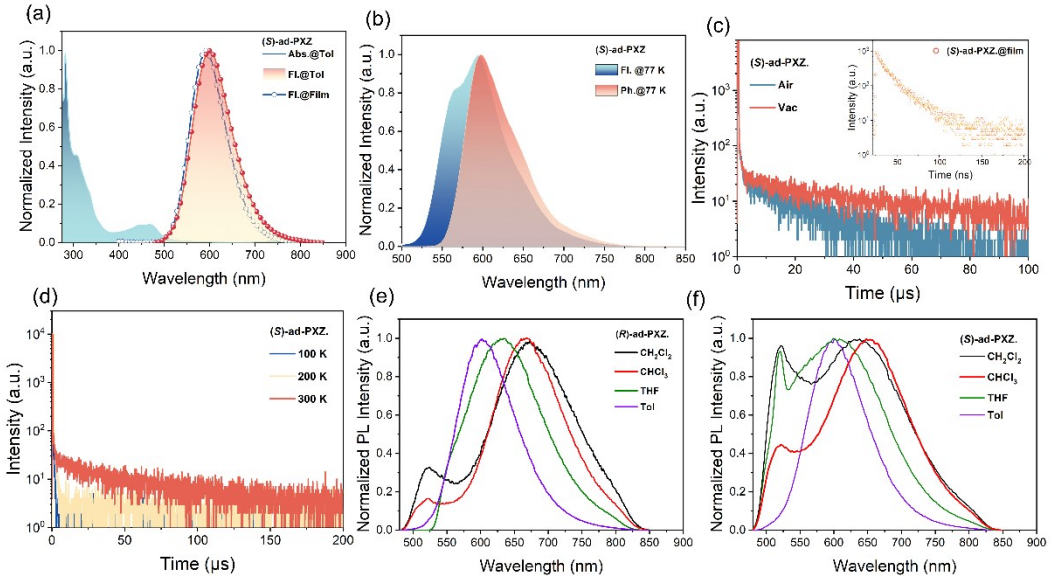

Fig S19. a) UV−vis absorption and PL spectra of **(*S*)-ad-PXZ** in toluene (10^{-5} M) and 10 wt % **(*S*)-ad-PXZ** doped film in TCTA (λ_{ex}=450 nm); b) Fluorescence and phosphorescence spectra of **(*S*)-ad-PXZ** in toluene at 77 K (λ_{ex}=450 nm); c) Transient PL spectra of the doped films of **(*S*)-ad-PXZ** in air and vacuum (Inset: prompt PL decay curves measured in a time window of 200 ns) (λ_{ex}=365 nm); d) Temperature-dependent transient PL decay spectra of the **(*S*)-ad-PXZ** doped film; (λ_{ex}=365 nm) e, f) The solvatochromism effect of **(*R*)-ad-PXZ/(*S*)-ad-PXZ** in different solvent.

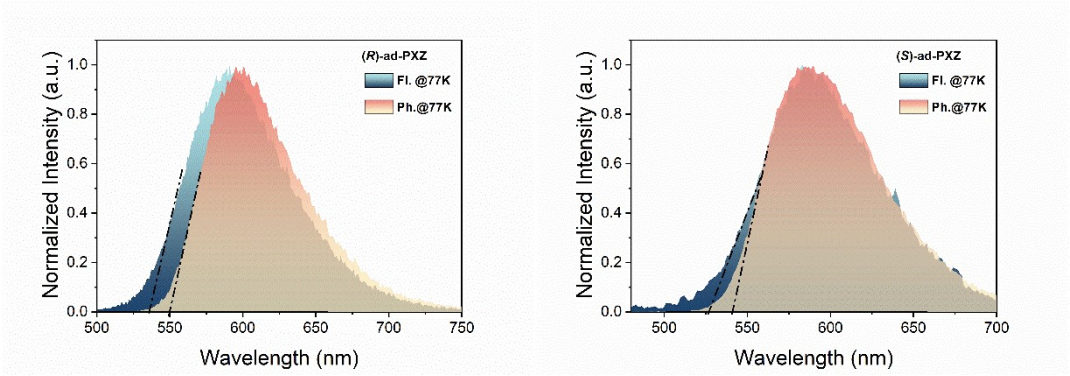

Fig S20 Fluorescence and phosphorescence spectra in 10 wt% doped films at 77 K (λ_{ex}=365 nm).

Table S1. Summary of photophysical and electrochemical properties of **(*R*)-ad-PXZ** and **(*S*)-ad-PXZ**

Compound	λ_{abs} [a] [nm]	λ_{em} [nm]	PLQY [b] [%]	τ_p [c] [ns]	τ_d [c] [μs]	φ_p [c] [%]	φ_d [c] [%]	HOMO/LUMO [d] [eV]	(ΔE_{ST}) [e] [eV]	g_{PL} [$\times 10^{-3}$]
(*R*)-ad-PXZ	295, 450	602 [a] 596 [b]	15.80	21	51.95	73	27	-4.86/-2.78	0.1	+2.8 [f] +5.8 [g]
(*S*)-ad-PXZ	295, 450	602 [a] 596 [b]	11.65	19	43.52	76	24	-4.81/2.73	0.1	-2.9 [f], -6.4 [g]

[a] in toluene (1.0×10^{-5} m) at room temperature. [b] 10 wt% **(*R*)-ad-PXZ//(*S*)-ad-PXZ** doped films in TCTA. [c] Prompt and delayed lifetime of the doped films in TCTA [d] HOMO level measured from the oxidation potential in 10^{-4} m acetonitrile solution by cyclic voltammetry with ferrocene as the internal standard, and LUMO level calculated from HOMO-E_g [e] Determined from fluorescence and phosphorescence emission spectra at 77 K in solution. [f] g_{PL} factors in toluene; [g] g_{PL} factors in doped film.

Electroluminescence performances

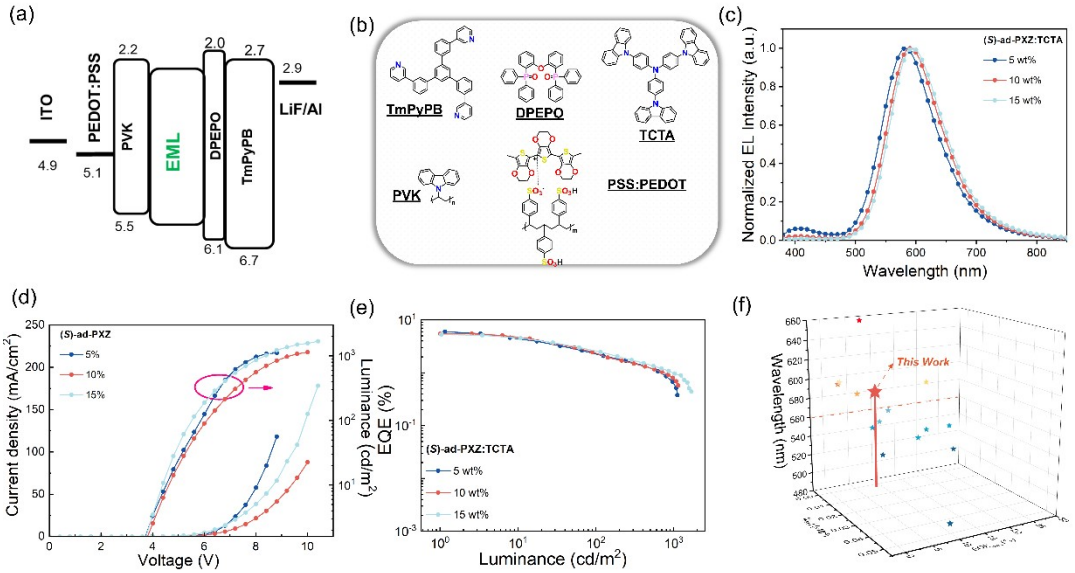

Fig S21. a) The structures of the solution-processable OLED materials; b) corresponding chemical structures of the used materials.c) normalized EL spectra of **(*S*)-ad-PXZ**; d) current density–voltage–luminance (J–V–L) characteristics; e) external quantum efficiency versus luminance (EQE–L) curves; f) Three-dimensional diagram summarizing the EQE, Wavelength and g_{EL} value of the representative solution-processed CP-OLEDs

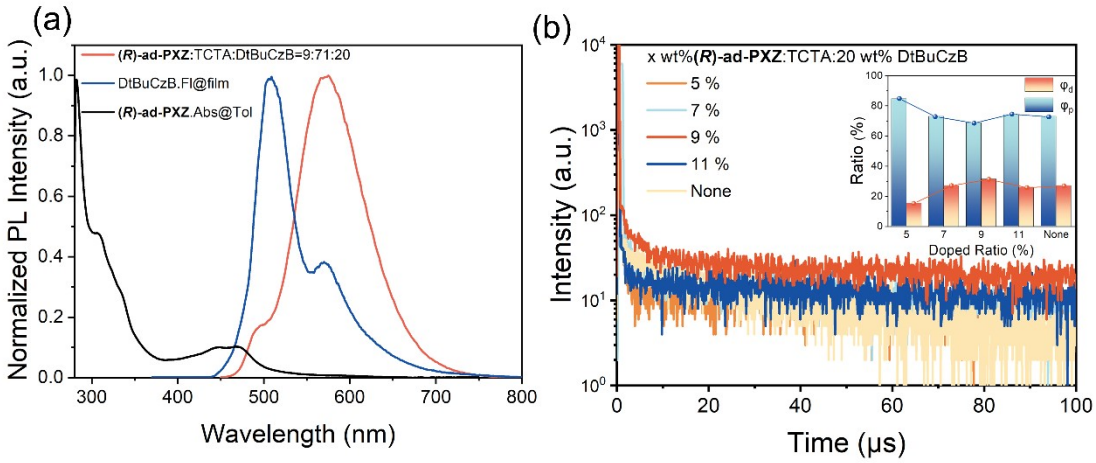

Fig S22 a) UV−vis absorption spectra of (R)-ad-PXZ in toluene and PL spectra of 9 wt % **(*R*)-ad-PXZ** with 20 wt% DtBuCzB in TCTA doped films (λ_{ex}=450 nm); b) Transient PL spectra of **(*R*)-ad-PXZ** with the different dopant sensitizer ratios (None, 5 wt%, 7 wt%, 9 wt%, 11wt%) (Inset: Red is the ratios of delayed components, blue is the proportion of prompt components);

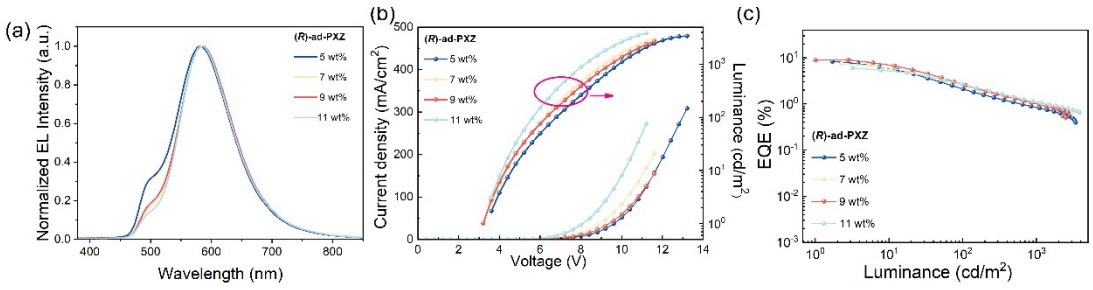

Fig S23. a) normalized EL spectra of X wt% **(*R*)-ad-PXZ** with 20 wt% DtBuCzB in TCTA doped films; b) current density–voltage–luminance (J–V–L) characteristics; c) external quantum efficiency versus luminance (EQE–L) curves

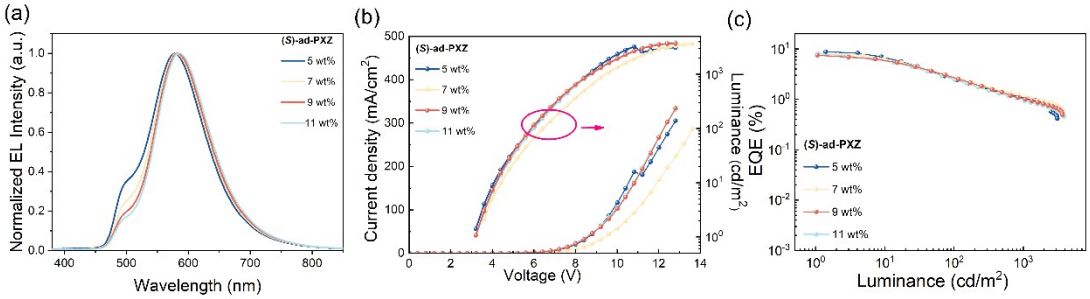

Fig S24 a) normalized EL spectra of X wt% **(S)-ad-PXZ** with 20 wt% DtBuCzB in TCTA doped films; b) current density–voltage–luminance (*J–V–L*) characteristics; c) external quantum efficiency versus luminance (*EQE–L*) curves;

Table S2. Summary of EL Performance of the best performance CP-OLED and TSCP-OLED using the **(*R*)-ad-PXZ** as the emitter.

Device	EML	V_{on} [a] [V]	L_{max} [b] [cd m^{-2}]	CE_{max} [c] [cd A^{-1}]	EQE_{max} [d] [%]	λ_{EL} [e] [nm]	CIE [f] [x, y]	g_{EL} [g] [×10^{-3}]
CP-OLED	**(*R*)-ad-PXZ:** TCTA	4.0	1385	12.83	5.8	588	(0.52, 0.47)	+1.4
TSCP -OLED	**(*R*)-ad-PXZ:** TCTA: DtBuCzB	3.2	2509	20.42	9.0	584	(0.57, 0.49)	+1.3

[a] V_{on}, the operating voltage at a brightness of 1 cd/m^2. [b] Maximum luminance [c] Maximum current efficiency. [d] Maximum external quantum efficiency. [e] Peaks of electroluminescence band. [f] Commission Internationale de L'Eclairage 1931 coordinates. [g] Electroluminescence dissymmetry factor.

Table S3. Summary of EL Performance of CP-OLED using diferrent dopant X wt % **(*R*)-ad-PXZ** and **(*S*)-ad-PXZ** in TCTA the as the emitter.

EML	Dopant [wt%]	V_{on} [a] [V]	L_{max} [b] [cd m^{-2}]	CE_{max} [c] [cd A^{-1}]	EQE_{max} [d] [%]	λ_{EL} [e] [nm]	CIE [f] [x, y]
(*R*)-ad-PXZ: TCTA	5	4.0	1434	12.87	5.1	574	(0.44,0.49)
	10	4.0	1385	12.83	5.8	588	(0.52,0.47)
	15	4.0	1469	7.83	3.9	594	(0.53,0.46)
(*S*)-ad-PXZ: TCTA	5	3.6	1112	14.36	6.0	582	(0.49,0.47)
	10	3.6	1141	11.67	5.5	592	(0.52,0.46)
	15	3.6	1683	10.39	5.3	594	(0.54,0.45)

[a] V_{on}, the operating voltage at a brightness of 1 cd/m^2. [b] Maximum luminance [c] Maximum current efficiency. [d] Maximum external quantum efficiency. [e] Peaks of electroluminescence band. [f] Commission Internationale de L'Eclairage 1931 coordinates.

Table S4. Summary of EL Performance of TSCP-OLED using diferrent dopant Xwt% **(*R*)-ad-PXZ** and **(*S*)-ad-PXZ** in TCTA as the emitter and 20 wt% DtBuCZB as the sensitizer.

EML	Dopant [wt%]	V_{on} [a] [V]	L_{max} [b] [cd m^{-2}]	CE_{max} [c] [cd A^{-1}]	EQE_{max} [d] [%]	λ_{EL} [e] [nm]	CIE [f] [x, y]
(*R*)-ad-PXZ: TCTA: 20 wt% DtBuCZB	5	3.6	3406	19.05	8.3	582	(0.47, 0.49)
	7	3.6	3049	17.17	7.4	584	(0.50, 0.48)
	9	3.2	2509	20.42	9.0	584	(0.57, 0.48)
	11	3.6	3843	14.07	6.0	584	(0.50, 0.48)
(*S*)-ad-PXZ: TCTA: 20 wt% DtBuCZB	5	3.2	3110	22.38	8.7	587	(0.46, 0.49)
	7	3.6	3645	20.00	7.8	580	(0.48, 0.49)
	9	3.2	3877	18.78	8.0	582	(0.49, 0.48)
	11	3.2	3674	17.42	7.5	586	(0.50, 0.48)

[a] V_{on}, the operating voltage at a brightness of 1 cd/m^2. [b] Maximum luminance [c] Maximum current efficiency. [d] Maximum external quantum efficiency. [e] Peaks of electroluminescence band. [f] Commission Internationale de L'Eclairage 1931 coordinates.